Proceedings of the Twenty-second (2012) International Offshore and Polar Engineering Conference
Rhodes, Greece, June 17–22, 2012

ISBN 978-1-880653-94–4 (Set); ISSN 1098-6189 (Set)

www.isope.org

Water Waves Generated by Moving Pressure Fields

Deniz Bayraktar Ersan and Serdar Beji
Istanbul Technical University, Faculty of Naval Architecture and Ocean Engineering
Maslak - Istanbul, Turkey

ABSTRACT

Boussinesq equations with improved dispersion characteristics are used to simulate the generation and propagation of waves due to moving pressure fields. With surface pressure terms in the momentum equations the numerical scheme is first run for a moving 3-D hemispherical pressure field for a range of Froude numbers. The wedge angles obtained from simulations are compared with the values calculated from the analytical formulas of Havelock. Furthermore, two ship-like slender pressure fields, representing a moving catamaran, are employed to visualize the interaction of the waves generated.

KEY WORDS: Boussinesq equations; Moving hemispherical pressure field; Moving catamaran; Wave pattern; Wedge angles

INTRODUCTION

The first depth-integrated nonlinear wave model that included the weakly dispersive effects as a non-hydrostatic pressure was derived by Boussinesq (1871) for constant water depth. Much later, Mei and LeMeháute (1966), and afterwards Peregrine (1967) derived Boussinesq equations for variable depth. While Mei and LeMeháute used the velocity at the bottom as the dependent variable, Peregrine used the depth-averaged velocity. Due to wide popularity of the equations derived by Peregrine, these equations are often referred to as the standard Boussinesq equations for variable depth in the coastal engineering community. To obtain a set of equations with better dispersion characteristics Madsen et. al (1991) and Madsen and Sørensen (1992) added higher-order terms with adjustable coefficients into the standard Boussinesq equations for constant and variable water depth, respectively. Beji and Nadaoka (1996) gave an alternative derivation of Madsen et. al's (1991) improved Boussinesq equations. Liu & Wu (2004) presented a model with specific applications to ship waves generated by a moving pressure distribution in a rectangular and trapezoidal channel by using boundary integral method. Torsvik (2009) made a numerical investigation on waves generated by a pressure disturbance moving at constant speed in a channel with a variable cross-channel depth profile by using Lynett et. al (2002) and Liu & Wu (2004)'s COULWAVE long wave model. All these works use the same type of cosine function to represent the moving surface object. In this study, besides a relatively simple hemispherical shape, a paraboloid-like function is used to model a moving catamaran type vessel.

BOUSSINESQ EQUATIONS WITH IMPROVED DISPERSION CHARACTERISTICS

In this work, Boussinesq equations as derived by Beji and Nadaoka (1996) are used with the addition of a pressure gradient to the momentum equation

$$\boldsymbol{u}_t + (\boldsymbol{u}\cdot\nabla)\boldsymbol{u} + g\nabla\eta = (1+\beta)\frac{h}{2}\nabla[\nabla\cdot(h\boldsymbol{u}_t)] + \beta g\frac{h}{2}\nabla[\nabla\cdot(\mathrm{h}\nabla\eta)] - (1+\beta)\frac{h^2}{6}\nabla(\nabla\cdot\boldsymbol{u}_t) - \beta g\frac{h^2}{6}\nabla(\nabla^2\eta) + \frac{\nabla \mathrm{p}}{\rho} \quad (1)$$

$$\frac{\partial\eta}{\partial t} + \nabla.[(h+\eta)\overline{\boldsymbol{u}}] = 0 \quad (2)$$

where β is a scalar set to $\beta=1/5$ according to the second order Padé expansion of the linear theory dispersion relation. Note that $\beta = 0$ corresponds to Peregrine's original equations. When $\beta = 1/5$ the model may propagate relatively shorter waves $(h/\lambda = 1)$ with acceptable errors in celerity where λ denotes wave length and h is the water depth.

NUMERICAL ALGORITM

Discretization of Governing Equations

The governing equations given by Equations (1) and (2) are discretized on an Arakawa staggered C-grid system as shown in Figure 1.

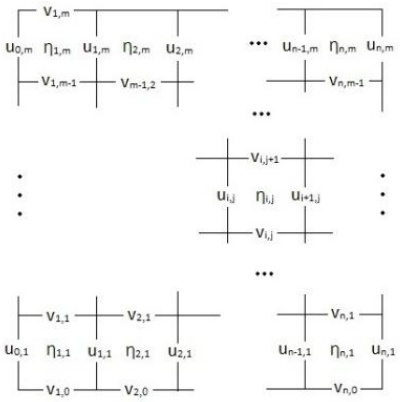

Figure 1: Location of dependent in Arakawa staggered C-grid system.

In the discretization process the continuity equation is substituted into the momentum equation in a way first used by O'Brien and Hurlburt (1972) for the solution of two-layer shallow water equations. Such an arrangement enables running the numerical scheme in the long wave mode besides the classical and improved Boussinesq modes. The continuity equation is then discretized as

$$\frac{n_{i,j}^{k+1}-n_{i,j}^{k}}{\Delta t}+\frac{1}{2}h\left[\left(\frac{\partial u}{\partial x}\right)^{k+1}+\left(\frac{\partial u}{\partial x}\right)^{k}\right]_{i-\frac{1}{2},j}= -\left[h_x u_{i-\frac{1}{2},j}^{k+\frac{1}{2}}+h_y v_{i,j-\frac{1}{2}}^{k+\frac{1}{2}}+\frac{\partial}{\partial x}(\eta u)^{k+\frac{1}{2}}+\frac{\partial}{\partial y}(\eta v)^{k+\frac{1}{2}}+h\frac{\partial v_{i,j-\frac{1}{2}}^{k+\frac{1}{2}}}{\partial y}\right] \quad (3)$$

where *i* and *j* denotes the spatial time steps in the *x* - and *y*- directions while *k* indicates the time level. Multiplying both sides by Δt and differentiating with respect to *x* gives

$$\left(\frac{\partial \eta}{\partial x}\right)_{i,j}^{k+1}=\left(\frac{\partial \eta}{\partial x}\right)_{i,j}^{k}-\frac{1}{2}h\left[\left(\frac{\partial^2 u}{\partial x^2}\right)^{k+1}+\left(\frac{\partial^2 u}{\partial x^2}\right)^{k}\right]_{i-\frac{1}{2},j}\Delta t -2h_x\left(\frac{\partial u}{\partial x}\right)_{i-\frac{1}{2},j}^{k+\frac{1}{2}}\Delta t-h_y\left(\frac{\partial v}{\partial x}\right)_{i,j-\frac{1}{2}}^{k+\frac{1}{2}}\Delta t -h_x\left(\frac{\partial v}{\partial y}\right)_{i,j-\frac{1}{2}}^{k+\frac{1}{2}}\Delta t-h\left(\frac{\partial^2 v}{\partial x\partial y}\right)_{i,j-\frac{1}{2}}^{k+\frac{1}{2}}\Delta t -\frac{\partial^2}{\partial x^2}(\eta u)_{i-\frac{1}{2},j}^{k+\frac{1}{2}}\Delta t-\frac{\partial^2}{\partial x\partial y}(\eta v)_{i,j-\frac{1}{2}}^{k+\frac{1}{2}}\Delta t \quad (4)$$

Likewise, multiplying equation (3) by Δt and differentiating with respect to y gives

$$\left(\frac{\partial \eta}{\partial y}\right)_{i,j}^{k+1}=\left(\frac{\partial \eta}{\partial y}\right)_{i,j}^{k}-\frac{1}{2}h\left[\left(\frac{\partial^2 v}{\partial y^2}\right)^{k+1}+\left(\frac{\partial^2 v}{\partial y^2}\right)^{k}\right]_{i-\frac{1}{2},j}\Delta t -2h_y\left(\frac{\partial v}{\partial y}\right)_{i-\frac{1}{2},j}^{k+\frac{1}{2}}\Delta t-h_x\left(\frac{\partial v}{\partial x}\right)_{i,j-\frac{1}{2}}^{k+\frac{1}{2}}\Delta t -h_y\left(\frac{\partial u}{\partial x}\right)_{i,j-\frac{1}{2}}^{k+\frac{1}{2}}\Delta t-h\left(\frac{\partial^2 u}{\partial x\partial y}\right)_{i,j-\frac{1}{2}}^{k+\frac{1}{2}}\Delta t -\frac{\partial^2}{\partial x\partial y}(\eta u)_{i-\frac{1}{2},j}^{k+\frac{1}{2}}\Delta t-\frac{\partial^2}{\partial y^2}(\eta v)_{i,j-\frac{1}{2}}^{k+\frac{1}{2}}\Delta t \quad (5)$$

Equations (4) and (5) are to be used in the discretized forms of the *x* – and *y*-components of the momentum equation, respectively. The *x*-component of the momentum equation is discretized as

$$\frac{u_{i,j}^{k+1}-u_{i,j}^{k}}{\Delta t}+\frac{1}{2}g\left[\left(\frac{\partial \eta}{\partial x}\right)^{k+1}+\left(\frac{\partial \eta}{\partial x}\right)^{k}\right]_{i+\frac{1}{2},j} =(1+\beta)\frac{h^2}{3}\left[\left(\frac{\partial^2 u}{\partial x^2}\right)^{k+1}-\left(\frac{\partial^2 u}{\partial x^2}\right)^{k}\right]\frac{1}{\Delta t} +(1+\beta)hh_x\left[\left(\frac{\partial u}{\partial x}\right)^{k+1}-\left(\frac{\partial u}{\partial x}\right)^{k}\right]\frac{1}{\Delta t}-(uu_x)^{k+\frac{1}{2}} -(vu_y)^{k+\frac{1}{2}}+(1+\beta)\frac{h^2}{3}v_{xyt}+\frac{1}{2}(1+\beta)hh_x v_{yt} +\frac{1}{2}(1+\beta)hh_y v_{xt}+g\beta\frac{h^2}{3}\eta_{xxx}+g\beta hh_x\eta_{xx} +g\beta\frac{h^2}{3}\eta_{xyy}+\frac{1}{2}g\beta hh_x\eta_{yy}+\frac{1}{2}g\beta hh_y\eta_{xy}\frac{1}{\rho}p_x \quad (6)$$

where the terms given in undiscretized form are to be discretized according to the Arakawa C-grid system at time level *k + 1/2*. Substituting $(\frac{\partial \eta}{\partial y})_{i,j}^{k+1}$ as given in Equation (4) into the above equation, multiplying by Δt and rearranging gives

$$h\left[\frac{1}{3}(1+\beta)h+\frac{1}{4}g\Delta t^2\right]\left(\frac{\partial^2 u}{\partial x^2}\right)^{k+1}+h_x\left[(1+\beta)h+\frac{1}{2}g\Delta t^2\right] =h\left[\frac{1}{3}(1+\beta)h-\frac{1}{4}g\Delta t^2\right]\left(\frac{\partial^2 u}{\partial x^2}\right) +h_x\left[(1+\beta)h-\frac{1}{2}g\Delta t^2\right]\left(\frac{\partial u}{\partial x}\right)-u_{i,j}^{k}+g\left(\frac{\partial \eta}{\partial x}\right)^{k} -\frac{1}{2}h_x\left[(1+\beta)h+\frac{1}{2}g\Delta t^2\right]\left(\frac{\partial v}{\partial y}\right)^{k+1} +\frac{1}{2}h_x\left[(1+\beta)h-\frac{1}{2}g\Delta t^2\right]\left(\frac{\partial v}{\partial y}\right)^{k} -\frac{1}{2}h_y\left[(1+\beta)h+\frac{1}{2}g\Delta t^2\right]\left(\frac{\partial v}{\partial x}\right)^{k+1} +\frac{1}{2}h_y\left[(1+\beta)h-\frac{1}{2}g\Delta t^2\right]\left(\frac{\partial v}{\partial x}\right)^{k} -h\left[\frac{1}{3}(1+\beta)h+\frac{1}{4}g\Delta t^2\right]\left(\frac{\partial^2 v}{\partial x\partial y}\right)^{k+1} +h\left[\frac{1}{3}(1+\beta)h-\frac{1}{4}g\Delta t^2\right]\left(\frac{\partial^2 v}{\partial x\partial y}\right)^{k} +\left[(uu_x)^{k+\frac{1}{2}}+(vu_y)^{k+\frac{1}{2}}\right]\Delta t -g\beta h\Delta t\left[\frac{h}{3}(\eta_{xxx}+\eta_{xyy})+h_x\left(\eta_{xx}+\frac{1}{2}\eta_{yy}\right)+\frac{1}{2}h_y\eta_{xy}\right] -\frac{1}{2}g\Delta t^2\left[\frac{\partial^2}{\partial x^2}(\eta u)^{k+\frac{1}{2}}+\frac{\partial^2}{\partial x\partial y}(\eta v)^{k+\frac{1}{2}}\right]-\frac{1}{\rho}p_x\Delta t \quad (7)$$

The y-momentum equation is obtained in exactly the same manner and therefore is not repeated here.

The numerical solution proceeds as follows. First, the provisional η values are computed from the continuity Equation (3) using the old time velocity values. The *x*- and *y*-momentum equations result in a tri-diagonal matrix system for the velocities *u* and *v* at the new time level. For the *x* -sweep, the new time level values u^{k+1}s are the only unknowns and are solved by Thomas Algorithm. Similarly for the *y*-sweep, the v^{k+1}s are the only unknowns to be solved. Finally the continuity equation is used again to obtain the corrected values of η using the last computed u^{k+1} and v^{k+1} values. At each time step the

procedure is iterated thrice, which is found to be sufficient for reliable results. For a better approach the successive values of the variables may be compared according to a convergence criterium. Nevertheless the numerical experiments show that the additional computational load is unnecessary as no appreciable improvement in the results is seen with increased iterations.

Boundary Conditions

All the boundaries surrounding the computational domain are specified as the radiation type boundary, across which the waves leave the domain without any reflection. For waves moving in a single direction Sommerfeld radiation condition reads for *u* and *v* respectively,

$$u_t + c_x u_x = 0 \qquad (8)$$
$$v_t + c_y v_y = 0$$

where c_x and c_y denote the *x* - and *y*-components of the phase celerity *c*. Numerical determination of c_x and c_y at every time step is not quite reliable therefore c is used in both cases, as is usually done. Higher-order boundary conditions as given by Enquist and Majda (1977) may also be used; however, the simpler Sommerfeld radiation condition is found to be acceptable.

2-D NUMERICAL SOLUTIONS

2-D simulations of waves (actually 3-D) generated by moving pressure fields are performed. First a 3-D hemispherical pressure field is used and the wedge angles computed from the numerical simulations for various depth Froude numbers are compared with the calculations from Havelock's theoretical formulas. Furthermore, two slender-body type pressure fields are used to show the interaction of the waves generated by a catamaran-like moving vessel.

Hemispherical Pressure Forcing

A hemispherical pressure field of the form

$$p(x,y) = p_0\sqrt{R^2 - x^2 - y^2} \qquad (9)$$

is used for the first simulation. Here p_0 is the peak value of the pressure distribution and *R* is the radius of the hemisphere. Figure 2 shows the hemispherical field. In the simulation *R* is taken as *40 m*, p_0 = *300 Pa*

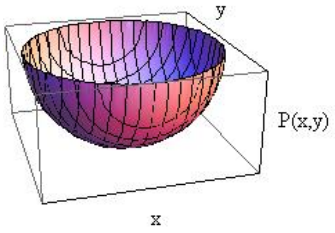

Figure 2: 3-D plot of the hemispherical pressure distribution.

and the water depth *h = 10 m* which gives $c = \sqrt{gh} = 10$ *m/s*. The simulation region is *2400 m × 1200 m* with $\Delta x = \Delta y = 4$ *m*. Time step is taken as $\Delta t = 0.2$ *s*. In the *x*-momentum equation $p_x = -xp_0/(R^2 - x^2 - y^2)^{1/2}$ and in the *y*-momentum $p_y = -yp_0/(R^2 - x^2 - y^2)^{1/2}$.

Figure 3 shows the contour plots of the simulated wave field at *t =10 s*, *20 s* and *48 s* for the depth-based Froude number $Fr = v/c = v/\sqrt{gh} = 1.1$, which corresponds the pressure field speed $v = 1.1\sqrt{gh} = 1.1c = 11$ *m/s*. It is to be noted that the wedge angle *65°* measured from the simulated wave field at *t = 90 s* is an acceptable approximation to the theoretical value of Havelock (1908) as can be seen in Table 1 and Figure 4.

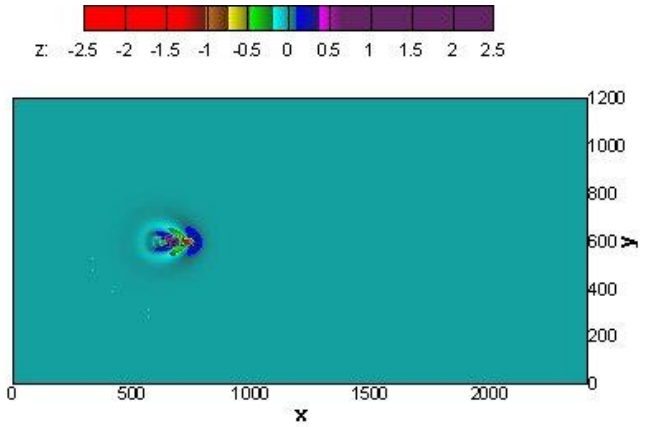

(a) t= 10 s, Fr=1.1

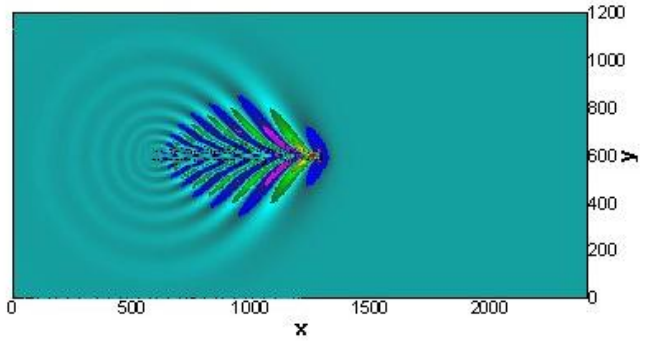

(b) t= 44 s, Fr=1.1

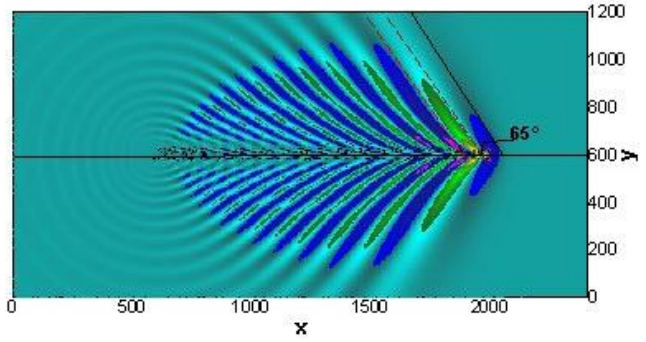

(c)t= 90 s, Fr=1.1

Figure 3: Wave contours of a moving hemisphere at different time steps using Boussinesq model with β = 1/5 for *Fr* = 1.1

Havelock (1908) investigated the wave patterns for subcritical and supercritical Froude numbers due to a moving surface pressure. For the wedge angle of a point impulse moving on water of finite depth Havelock gives

$$\alpha = \arccos\sqrt{8(1-n)}/(3-n) \quad \text{if} \quad Fr \le 1$$
$$\alpha = \arcsin\sqrt{p} \quad \text{if} \quad Fr > 1$$

where $p = gh/v^2 = c^2/v^2 = 1/Fr^2$. For a given Froude number or *p* in the subcritical range, first *kh* is solved by iteration from the relationship $m(3 - n) = 2/p$ where $m = \tanh kh/kh$ and $n = 2kh/\sinh 2kh$. Then,

using the computed *kh* the numerical value of *n* is obtained to compute *α*. For the supercritical range is a function of *p* alone therefore no additional computation is needed. The tabular form of the numerically and analytically computed wedge angles for the Froude numbers considered are given in Table 1. It should be mentioned that some limited number of numerical values given by Havelock does not exactly match with their counterparts in Table 1, as the present table is compiled by high-accuracy computations.

Table 1: Comparisons of numerically obtained wedge angles with Havelock's analytical results for a range of depth-based Froude numbers.

Wedge Angle			
Fr	**Boussinesq (Numerical)**	**Havelock (Analytical)**	**Relative Error Percentage (%)**
0.63	18.00	19.69	8.58
0.70	20.00	20.26	1.29
0.75	21.00	21.10	0.47
0.86	25.00	25.36	1.43
0.90	25.00	28.50	12.28
0.96	40.00	37.78	5.86
0.97	40.00	40.69	1.69
0.98	39.00	44.66	12.68
0.99	48.00	51.01	5.90
1.01	82.00	81.93	0.08
1.05	72.00	72.25	0.34
1.10	65.00	65.38	0.58
1.20	54.00	56.44	4.33
1.30	47.00	50.28	6.53
1.40	43.00	45.58	5.67
1.50	42.00	41.81	0.45
1.60	36.00	36.03	0.09
1.80	33.00	33.75	2.22
2.00	30.00	30.00	0.00

It is to be noted that in the subcritical range as Froude number approaches zero the relative depth *kh* becomes larger. On the other hand, in the entire supercritical range *kh* assumes the limiting case of zero and disappears from the wedge angle computations. Thus, in a sense, low Froude numbers represent relatively deep waters while high Froude numbers correspond to very shallow waters. For *Fr = 0* Kelvin's well-known result of a deep-water wedge angle $\alpha = 19^{o}28'$ is obtained as may be seen in Figure 4 where the wedge angles computed from Havelock's analytical formulas and measured from the graphs of the numerical solutions of the present Boussinesq model are shown. It must be noted that since the Froude number mentioned here is depth based ($Fr = v/\sqrt{gh}$), *Fr = 0* corresponds to the deep water case where h is theoretically infinite while $v \neq 0$. Therefore, it is possible to say that in Figure 4, *Fr<1* represents the deep water zone and *Fr*>1 the shallow water zone. Since the Boussinesq equations in general are applicable to intermediate and shallow water waves, in this work the subcritical range for the simulations is selected between *Fr=0.63* and *Fr=0.99* as shown in Table 1.

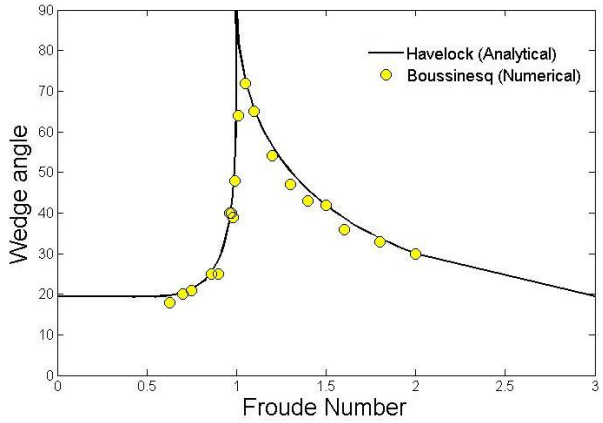

Figure 4: Comparison of numerically obtained wedge angles with Havelock's theoretical formulas

Finally, perspective views of two slender-body shaped pressure fields representing a moving catamaran-like vessel are given in Figure 5 for *Fr = 0.97* at *t=9 s* and *t=18 s* respectively.

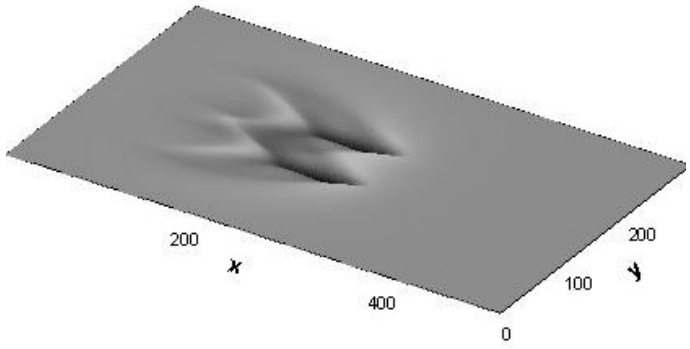

(a) t = 9 s for Fr = 0.97

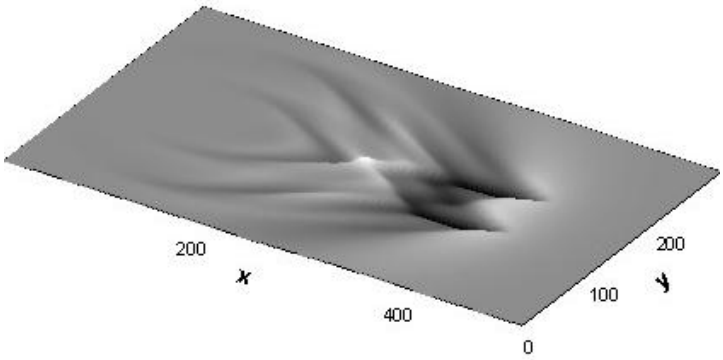

(b) t = 18 s for Fr = 0.97

Figure 5: Perspective views of two slender body shaped pressure fields representing a moving catamaran type vessel

CONCLUSIONS

Boussinesq equations are usually employed for modeling nearshore waves or waves in intermediate water depths. Besides these applications, the Boussinesq equations may also be employed to model wave generation and propagation by moving surface disturbances. The surface disturbance may come from a moving free surface object which is associated with a moving surface vessel. By adding a moving surface pressure into Boussinesq equations, the wave patterns for different depth based Froude numbers are investigated for a hemispherical type pressure field. The computed wedge angles are compared with calculations from Havelock (1908)'s analytical results. Comparisons reveal good agreement with the theory, especially for supercritical Froude numbers, $Fr \geq 1$, where the relative depth is small. In the subcritical range, $Fr \leq 1$, the average error percentage between the computed and the theoretical values is around *5.58 %*, considerably greater than those of the supercritical range, which is on the average *2.03 %*. The reason for this asymmetry in average error percentages between sub- and supercritical Froude numbers is probably due to the depth limited character of the Boussinesq equations. As indicated before, the subcritical range indicates relatively greater depths with completely deep water for zero Froude number. Therefore, the relatively poor performance of the numerical model in the subcritical range may be attributed to the deep water characteristics of the waves generated. Finally, two slender body shaped pressure fields are used for visual demonstration purpose of waves due to a catamaran-like surface object.

REFERENCES

Beji, S. and Nadaoka, K. A. (1996). "Formal Derivation and Numerical Modelling of the Improved Boussinesq Equations for Varying Depth," *Ocean Engineering.,*Vol. 23, pp 691.

Boussinesq, J.V. (1872). "Theory of waves and surges which propagate the length of a horizontal rectangular canal, imparting to the fluid contained within the canal velocities that are sensibly the same from the top to the bottom," *J. Math. Pures and Appl.*, Vol. 17, pp 55–108.

Engquist, B. and Majda, A. (1977). "Absorbing Boundary Conditions for the Numerical Simulations of Waves," *Mathematics of Computation*, Vol. 31, Number 139, pp. 629-651.

Havelock, T., (1908). "The propagation of groups of waves in dispersive media with application to waves on water produced by a travelling disturbance," *Proceedings of the Royal Society of London*, Vol. 81(549), pp 398–430.

Liu, P.L.F and Wu, T.R. (2004). "Waves Generated by Moving Pressure Disturbances in Rectangular and Trapezoidal Channels," *J. Hydraul. Res.*, Vol. 42, pp 163.

Lynett, P., Wu, T.-R., and Liu, P. L.-F. (2002). "Modeling Wave Runup with Depth-Integrated Equations," *Coastal Eng.*, Vol. 46, pp 89.

Madsen, P. A., Murray, R. and Sørensen, O. R. (1991). "A New Form of the Boussineq Equations with Improved Linear Dispersion Characteristics," *Coastal Engineering.,*Vol. 15, pp 371.

Madsen, P. A. and Sørensen, O. R. (1992). "A New Form of the Boussineq Equations with Improved Linear Dispersion Characteristics Part 2," *Coastal Engineering.,*Vol. 18, pp 183.

Mei, C.C. and LeMehaute, B. (1966). "Note on the Equations of Long Waves Over an Uneven Bottom," *J. Geophys. Res.,*Vol. 71, pp 393.

Nwogu, O. (1993). "Alternative Form of Boussinesq Equations for Nearshore Wave Propagation," *Journal of Waterway, Port, Coastal and Ocean Engineering*. Vol. 119, pp 618.

O'Brien, J.J. and Hurlburt, H.E. (1972). "A Numerical Model of Coastal Up-welling," *Journal of Physical Oceanography*, Vol. 2, pp 14-26.

Peregrine, D. H. (1967). "Long Waves on a Beach" *J. Fluid Mech.,*Vol. 27, pp 815.

Torsvik, T., Pedersen, G. and Dysthe, K. (2009). "Waves Generated by a Pressure Disturbance Moving in a Channel with a Variable Cross-Sectional Topography," *Journal of Waterway, Port, Coastal and Ocean Engineering,*Vol. 135, pp 120-123.